Proceedings of the 28th AIAA/CEAS Aeroacoustics 2022 Conference, 14-17 June, Southampton, UK
DOI:10.2514/6.2022-2935

Flow and Noise Predictions of the Isolated Subsonic Jets from the Doak Laboratory Experiment

Vasily Gryazev,[1] Annabel P. Markesteijn[2], Sergey A. Karabasov[3]
Queen Mary University of London, London, E1 4NS, UK,

Jack L. T. Lawrence[4]
University of Southampton, Southampton, SO17 1BJ, UK

Anderson Proença[5]
Cranfield University, Cranfield, MK43 0AL, United Kingdom

Abstract

Flow and noise solutions using Large Eddy Simulation (LES) are evaluated for two jets at acoustic Mach numbers 0.6 and 0.8. The jets correspond to Doak Laboratory Experiment performed at the University of Southampton. LES method is based on the Compact Accurately Boundary-Adjusting High-Resolution Technique (CABARET) scheme and is implemented on Graphics Processing Units. In comparison with many other jet noise benchmarks, the Doak jet cases include well-defined boundary conditions corresponding to the meanflow velocity and turbulent intensity profiles measured just downstream of the nozzle exit. The far-field noise predictions are obtained using two approaches. First, the LES solutions are coupled with the penetrable surface formation of the Ffowcs Williams–Hawkings method. The second approach is based on the reduced-order implementation of the Generalised Acoustic Analogy model for which time averaged quantities are obtained from the LES solutions. All numerical solutions are compared with the flow and acoustic microphone measurements from the Doak experiment. The results are cross-validated using the sJet code, which corresponds to an empirical model obtained from interpolations over a large set of NASA jet noise data.

I. Introduction

Despite decades of research, jet noise remains an active area in aeroacoustics [1-5]. Due to advances in high-resolution algorithms and computer architectures, Large Eddy Simulations (LES) have become increasingly popular for high-resolution jet flow and noise calculations. In our previous works, we developed a high-resolution Large Eddy

[1]Post-Doctoral Researcher, School of Engineering and Material Sciences, Mile End Road, London, E1 4NS, UK.
[2]Post-Doctoral Researcher, School of Engineering and Material Sciences, Mile End Road, London, E1 4NS, UK; also Research Scientist/Director, GPU-Prime Ltd., 16 St. Thomas Close, Comberton, Cambridge, England CB23 7DN, United Kingdom. Member AIAA.
[3]Professor, School of Engineering and Material Sciences, Mile End Road London, E1 4NS, UK; also Research Scientist/Director, GPU-Prime Ltd., 16 St. Thomas Close, Comberton, Cambridge, England CB23 7DN, United Kingdom. Associate Fellow AIAA.
[4]Research Fellow, Institute of Sound and Vibration Research, Highfield, Southampton SO17 1BJ, Member AIAA.
[5]Research Fellow in Experimental Aerodynamics, School of Aerospace, Transport and Manufacturing, Cranfield, MK43 0AL, Member AIAA.

Simulations solver based on the Compact Accurately Boundary-Adjusting high-REsolution Technique (CABARET) method [6-8]. CABARET is a shock-capturing scheme with improved dissipation and dispersion properties and implemented with asynchronous time stepping [9]. All simulations correspond to the Monotonically Integrated LES (MILES) framework implemented on Graphics Processing Units (GPU) to speed up the solution turn-around time to 2-3 days on LES grids 100-120 million cells [10-13]. A wall model and synthetic turbulence inflow conditions are used to model the upstream flow development inside the nozzle [13]. For the current simulations, the conditions of a recent single-stream jet experiment campaign conducted in the Doak Laboratory at the University of Southampton are considered [3-5]. The jet issues from a convergent profiled nozzle at an acoustic Mach number of 0.6 and 0.8 and a Reynolds number around one million.

Notably, in comparison with the previous jet flow and noise simulations performed with the CABARET method, here we managed to tailor the inflow jet boundary conditions to accurately represent both the time-averaged velocity and the turbulence intensity profiles measured just downstream of the nozzle exit. The OpenFOAM snappyHexMesh utility is used for generating patches of high-quality Cartesian grid locally refined in the location of early shear layers. For far-field noise calculations, the penetrable-surface formulation of the Ffowcs Williams-Hawkings (FW-H) method [14] with multiple closing disks is applied.

The first goal of this work is to explore the capability of our high-fidelity GPU LES solver coupled with the FW-H method for accurate noise spectra calculations up to frequencies corresponding to the jet Strouhal number of about 10 in a wide range of observer angles for the benchmark jet noise problem, which includes well-defined boundary conditions. In addition to the Doak jets, the results will be cross validated in comparison with the NASA sJet model [15], which corresponds to an empirical model obtained from interpolations over a large set of NASA jet noise data.

The second goal is to calculate the far-field noise of the same Doak jets by applying a reduced-order acoustic analogy model based on simple time-averaged flow properties and turbulence kinetic energy extracted from the LES. Specifically, following Goldstein [16-18] we consider the most advanced formulation from the class of acoustic analogies — the Generalised Acoustic Analogy (GAA). For cold jet noise modelling in the framework of GAA, directivities of the effective source term (e.g., the relative amplitudes of co-variance of fluctuating Reynolds stresses) are modelled using LES following [19-21].

II.Experimental Setup

The Institute of Sound and Vibration Research (ISVR) Doak Laboratory is an anechoic chamber, fully anechoic down to a frequency of 400 Hz. The facility has dimensions approximately of 15 m length by 7 m width by 5 m height. A core air jet is supplied by a high-pressure compressor–reservoir system. Single-stream jet measurements can be performed on flow regimes characteristic of civil aircraft and for 1⁄50th-scale experiments. The jet rig can achieve a controlled exit acoustic Mach number range of between 0.15 and 1. Further information regarding the Doak Flight Jet Rig (FJR) can be found in [3-5] and photographs of the Doak FJR facility are shown in Fig.1.

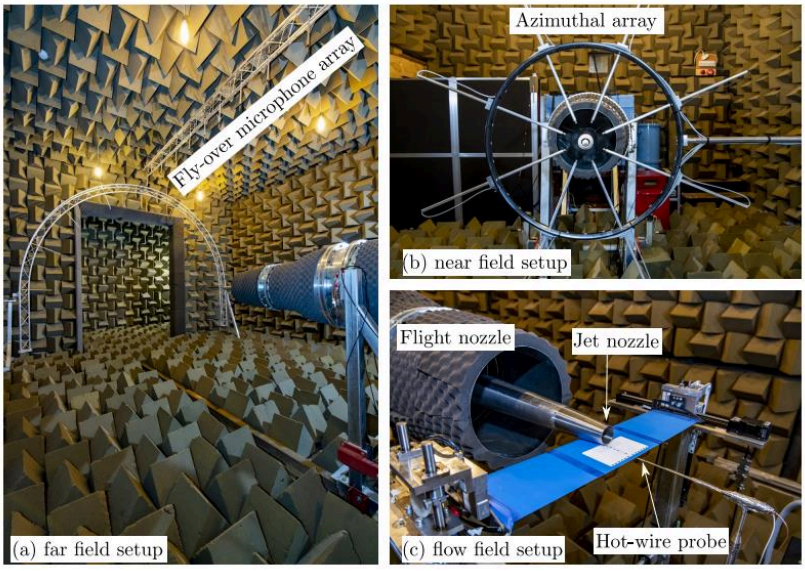

Fig.1 Photographs of the Flight Jet Rig in the Doak Laboratory at the University of Southampton

III. Flow Solution

The jet cases considered in this work are both isothermal and operate at acoustic Mach number $\mathrm{Ma} = 0.6$ and $\mathrm{Ma} = 0.8$ using CABARET Wall Modelled LES. The jet nozzle wall geometry is included in the computational domain, which includes several areas of refinement. The stream-wise extent of the computational domain is about $100D_j$ and the radial size is $30D_j$.

Following [22], in order to simulate the turbulent inflow boundary condition at the inlet of the computational domain upstream of the nozzle exit, a synthetic turbulence condition is implemented in the CABARET method using the off-the-shelf synthetic turbulence generator by [23-24]. Briefly, the von-Karman Pao wavenumber spectrum of the turbulent kinetic energy is used. The number of cells and wave forms in each direction of the turbulence box is adjusted so that the generated turbulent structures are sufficiently resolved on the LES grid near the wall. The magnitude of the input wavenumber spectrum and the location of the velocity distribution in a cross-stream frame of the box are adjusted so that turbulence intensity and velocity profile upstream of the hump agree with the measurements for both the jet cases (Fig.2). For wall modelling, the size and thickness of the layers near the boundary can be precisely controlled in the framework of the OpenFOAM snappyHexMesh routine, which involves adding body-fitted hexahedral layers near the viscous wall boundary. During the automatic meshing procedure, the distance between the centres of control volumes close to the boundary and the boundary itself is kept within a prescribed distance. Following [13, 22] the so-called equilibrium wall model is considered. The basic steps of the WMLES algorithm are implemented as follows. Inside the boundary layer mesh, each time step the cell centred values of the velocity and density are evaluated. These values are provided to the wall model, which, in turn, provides the wall shear stress. Consequently, this wall shear stress is used as a boundary condition for the LES at the wall. The wall model is based on the algebraic method using Reichardt's law as described in [25]. Reichardt's law of the wall gives a relation between the local u+ and the y+ of the wall, where in the WMLES calculation the instantaneous velocity is used as input to the wall law. The resulting non-linear algebraic equation for the velocity profile is solved by a simple Newton iteration, giving the wall shear stress at a negligible cost compared to the LES time step. At the external boundaries characteristic non-reflecting boundary conditions were applied along with the grid stretching similar to the previous CABARET jet calculations [13].

For the Ma = 0.8 case, the mesh resolution near the nozzle exit is $dx / D_j = 0.004$, $dy / D_j = 0.002$, and $dz / D_j = 0.004$. The mesh resolution near the end of the potential core is $dx / D_j = 0.015$, $dy / D_j = 0.015$, and $dz / D_j = 0.015$. This leads to the overall mesh count of 137 million cells. Images of the mesh in the jet symmetry plane are shown in Fig.3. Initially, the same mesh was used for the $\mathrm{Ma} = 0.6$ case as for the $\mathrm{Ma} = 0.8$ jet, however, it was noticed that due to a lower jet velocity, the former jet spreads faster, thereby leading to wider shear layers. Hence, the original LES grid for the $\mathrm{Ma} = 0.6$ was adapted. The modified mesh follows the same logic as the mesh for the $\mathrm{Ma} = 0.8$ case, with two exceptions. To adapt for a wider shear layer spreading of the slower jet, additional mesh refinement is applied at a larger radius corresponding to the outer shear layers. In addition, since it is known that the development of jets with wider initial shear layers may become sensitive to the turbulent inflow boundary condition [26], an additional effort was devoted to further locally refine the boundary layer grid inside the nozzle and in the early shear layer region in all 3 directions by a factor of 3. At the same time, to partly balance the grid size increase, a shorter section of the upstream nozzle geometry was simulated by imposing appropriate synthetic turbulent inflow boundary conditions closer to the nozzle exit in comparison with the $\mathrm{Ma} = 0.8$ case. Overall, this led to an increase of the LES grid for the $\mathrm{Ma} = 0.6$ case to 196 million cells.

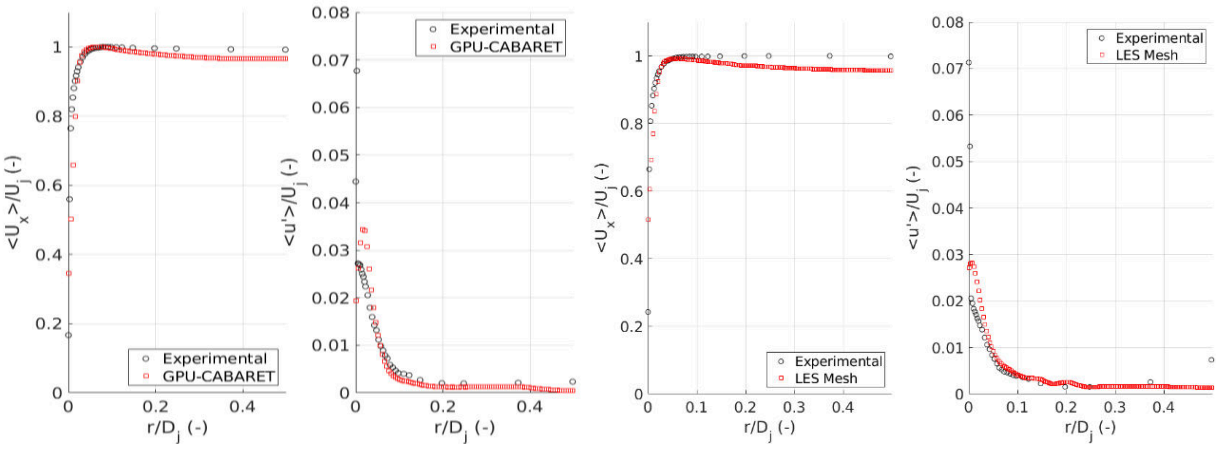

(a) (b)

Fig.2 Comparison of the inflow profiles at the nozzle exit obtained from LES with the experiment: mean axial velocity and mean axial velocity fluctuations for Ma = 0.6 (a) and Ma = 0.8 (b) jet cases.

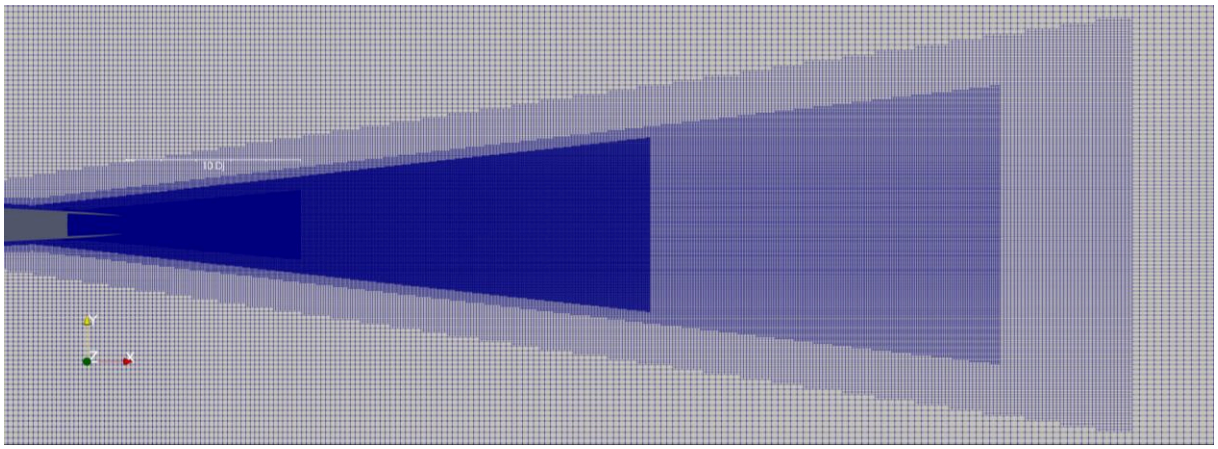

(a)

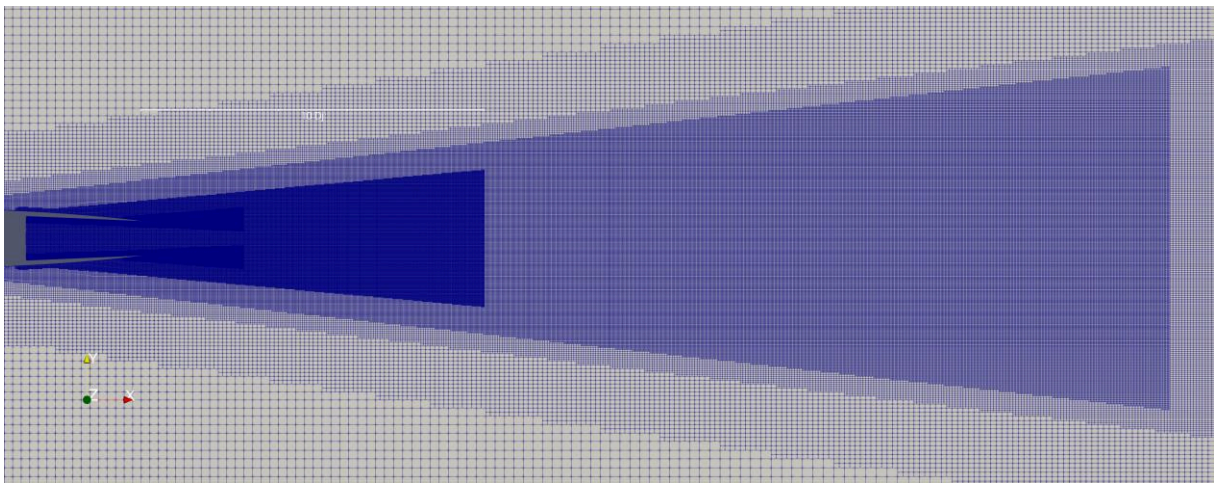

(b)

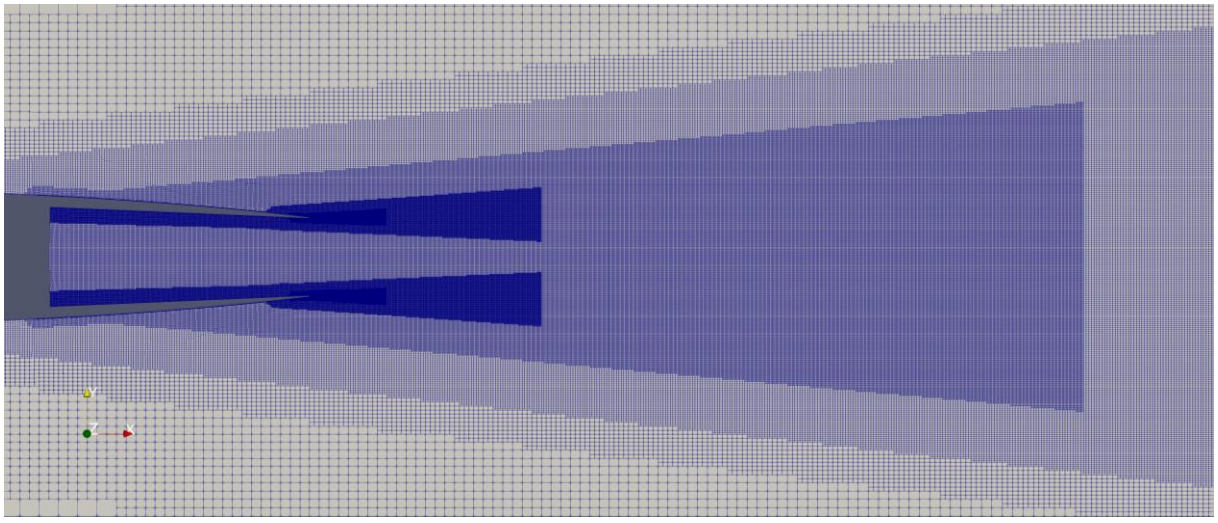

(c)

Fig.3 A series of zoomed-in images of the LES mesh in the jet symmetry plane for Ma=0.80 case – from (a) to (c). Notice the area of refined mesh inside the nozzle.

Figures 4-7 show the comparison of the LES solution with the experimental data. Radial profiles of the axial mean flow velocity and axial velocity fluctuations are shown for $\mathrm{Ma} = 0.6$ and $\mathrm{Ma} = 0.8$ jet cases. For the $\mathrm{Ma} = 0.6$ an overall good agreement is obtained for both the meanflow velocity distributions and turbulent velocity fluctuations. Some discrepancies are noticeable close to the jet centreline, where LES seems to underpredict turbulent mixing compared to the experiment as well as at further downstream locations of the jet, where the LES tends to overpredict the potential core length. The comparison between the LES results and the experiment for the $\mathrm{Ma} = 0.8$ jet is more-or-less similar to the $\mathrm{Ma} = 0.6$ case apart from larger discrepancies around the jet centre line. Notably, as our tests confirmed, the discrepancies near the centreline between the LES and the experiment are insensitive to the LES grid density in this region. Hence, these differences may originate from the intrusive measurement procedure used in the experiment, where the probes immersed in the flow trigger additional jet mixing, and which effect was not accounted for in the LES model. Notably, the differences of the implemented inflow boundary conditions in the LES from the experimentally realised ones (e.g. due to turbulence anisotropy effects at the nozzle exit) are less likely to be an issue because the LES-based noise spectra predictions are in excellent agreement with the acoustic measurements, once the probes were removed from the jet.

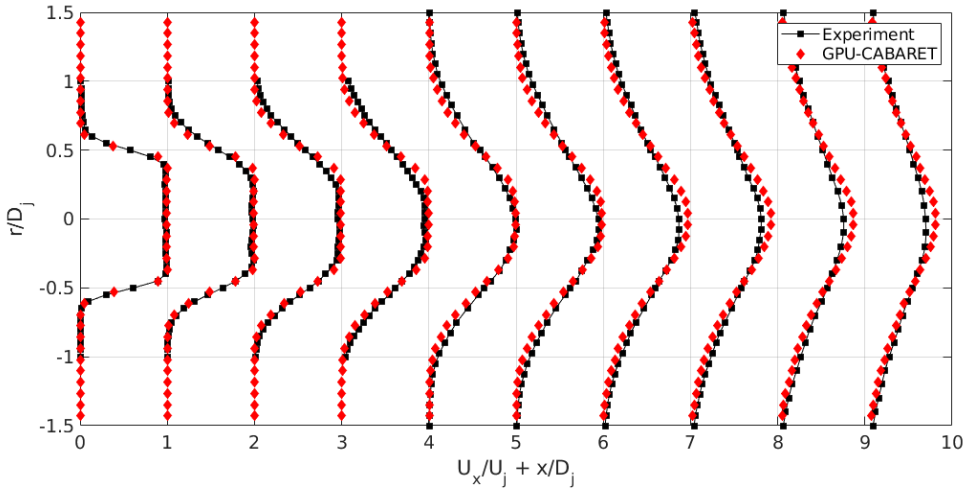

Fig.4 Radial profiles of mean axial velocity compared to experimental results for the Ma=0.6 case

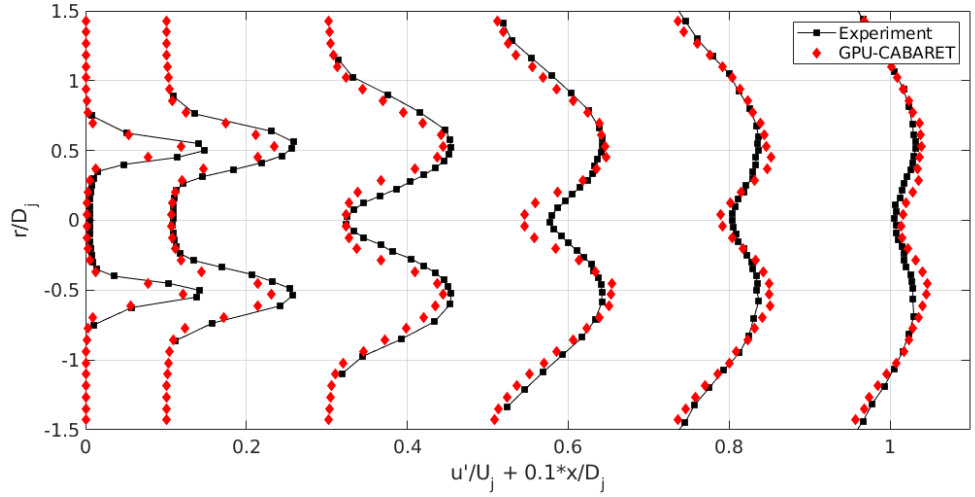

Fig.5 Radial profiles of the rms of axial velocity compared to experimental results for the Ma=0.6 case

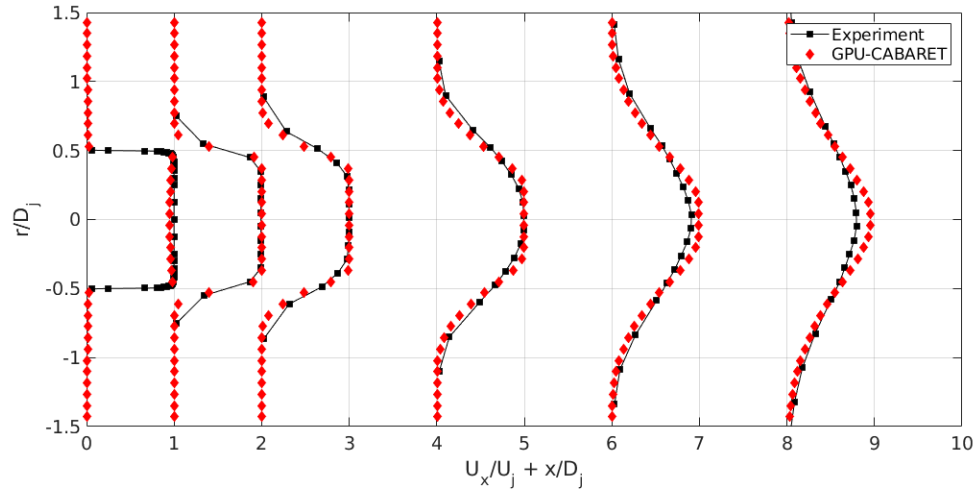

Fig.6 Radial profiles of mean axial velocity compared to experimental results for the Ma=0.8 case

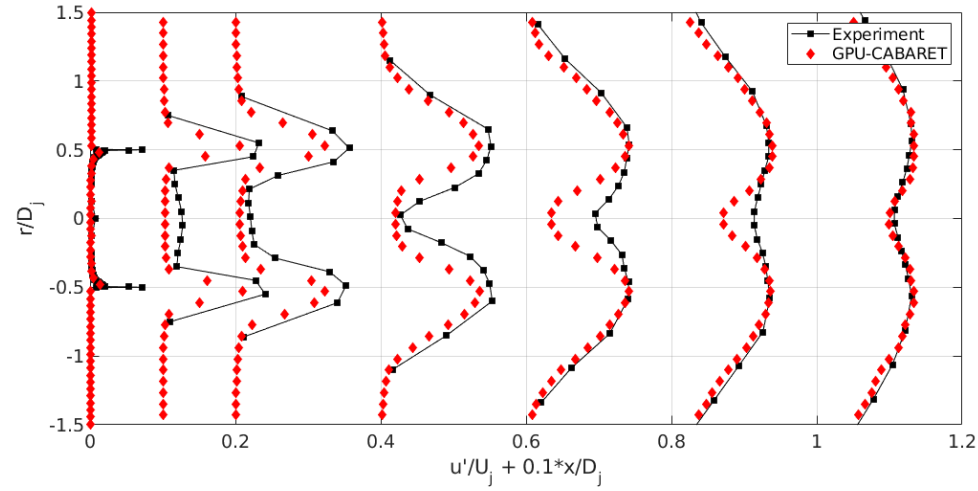

Fig.7 Radial profiles of the rms of axial velocity compared to experimental results for the Ma=0.8 case

Both LES meshes were run on a workstation with 2x NVIDIA RTX A6000 GPUs. As these GPUs have 48GB of memory, one such workstation is able to simulate a 260 million LES case with GPU CABARET within less than 6 days as the time to solution. The total Time Units (TUs) per hour for the Ma = 0.6 and Ma = 0.8 were similar, as the asynchronous time stepping algorithm implemented in CABARET ensured the added boundary layers for the Ma=0.6 case did not increase the computation time considerably despite the explicit time step. One TU corresponds to the time taken for a turbulence eddy moving with the jet speed to pass the distance equal to the nozzle diameter. The amount of TUs per day obtained on the 2 GPU were 100 for the Ma = 0.6 case and 150 for the Ma = 0.8 case. A total of 300 TUs for initialisation run plus 500 TUs for statistics were computed for the Ma = 0.6 case and 300 plus 1100 TUs were computed for the Ma = 0.8 case.

IV.Acoustic Modeling Methods

For the far-field noise calculations, the standard penetrable-surface formulation of the Ffowcs Williams-Hawkings method [14] is applied. Following the previous experience with static single-stream jet noise calculations with GPU CABARET [13], a conical acoustic control surface was used with closing discs [27] placed in the downstream direction from 25 to 32 nozzle diameters downstream of the nozzle exit. For computing the spectra from the time signal, the standard Welch method of Fourier transforms of short periodograms is used, which implementation details can be found in [13]. In accordance with the mesh design, the FW-H surface resolution near nozzle exit corresponds to the maximum resolved Strouhal number, $St_D = 11$ based on 8 PPW (Points Per acoustic Wavelengths) while it is $St_D = 2$ near the end of the FW-H surface. Here and in other places the Strouhal number is defined on the nozzle exit diameter and jet velocity, $St_D = fD_j / U_j$.

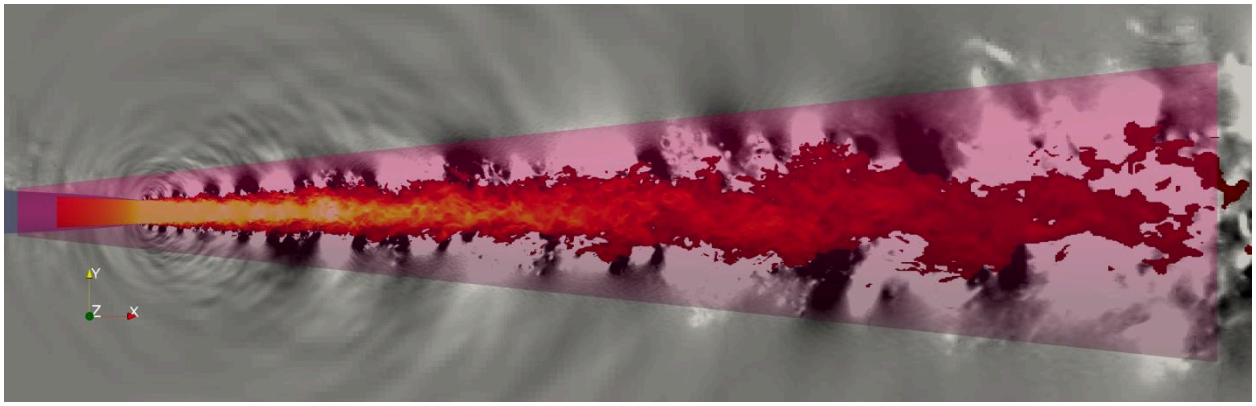

Fig.8 The instantaneous velocity contours (scale 0 to 310 m/s) and the pressure waves (scale -100Pa to 100Pa from p0). The FW-H surface is also shown. The region near the end has 16 closing discs spaced over a distance of 10 jet diameters.

In addition, the GAA model is implemented for acoustic predictions of the same jets. In accordance with the GAA model [17], the power spectral density of the far-field pressure signal can be expressed as the following convolution integral of the source term with the propagator function:

$$S(\mathbf{x},\omega) = \int_V \int_V \hat{R}_{ijkl}(\mathbf{y},\boldsymbol{\Lambda},\omega)\hat{I}_{ij}(\mathbf{y},\omega;\mathbf{x})\hat{I}^*_{kl}(\mathbf{y}+\boldsymbol{\Lambda},\omega;\mathbf{x})d\boldsymbol{\Lambda}d\mathbf{y}, \tag{1}$$

where $\hat{R}_{ijkl}(\mathbf{y},\boldsymbol{\Lambda},\omega)$ is the Fourier transform of the generalised stress tensor auto-covariance term, so that

$$\hat{R}_{ijkl}(\mathbf{y},\boldsymbol{\Lambda},\omega) = \int_{-\infty}^{\infty} R_{ijkl}(\mathbf{y},\boldsymbol{\Lambda},\tau)e^{i\omega\tau}d\tau, \text{ where } R_{ijkl}(\mathbf{y},\boldsymbol{\Lambda},\tau) = \overline{T'_{ij}(\mathbf{y},t)T'_{kl}(\mathbf{y}+\Delta,t+\tau)}, \tag{2}$$

the overbars stand for averaging over time t and $i,j,k,l = 1,2,3$. And the corresponding stress term is defined as

$$T'_{ij} = \left(\rho v'_i v'_j - \overline{\rho} v'_j v'_j\right), \; i,j,k,l = 1,2,3 \tag{3}$$

The components of the second-rank wave-propagation tensor of the sound integral (1) are defined by

$$\hat{I}_{ij}(\mathbf{y},\omega\,|\,\mathbf{x}) = \frac{\partial \hat{v}_j^{(a)}(\mathbf{y},\omega\,|\,\mathbf{x})}{\partial y_i} - \left[\frac{\partial \tilde{v}_j}{\partial y_i}(\mathbf{y})\, p^{(a)}(\mathbf{y},\omega\,|\,\mathbf{x}) + \tilde{v}_j \frac{\partial p^{(a)}(\mathbf{y},\omega\,|\,\mathbf{x})}{\partial y_i}\right] \tag{4}$$

$$+\frac{\delta_{ij}}{2}\left(i\omega + \tilde{v}_k \frac{\partial}{\partial y_k}\right) p^{(a)}(\mathbf{y},\omega\,|\,\mathbf{x}),$$

The adjoint vector Green's function is obtained by solving the locally parallel flow equations with the coefficients defined from the LES meanflow solution which details can be found in [19, 21, 28].

A simple exponential-Gaussian model is used following the works of [19,21, 29].

$$R_{ijkl}(\mathbf{y},\boldsymbol{\Delta},\tau) = A_{ijkl}(\mathbf{y})\exp\left[-\frac{|\Delta_1|}{\tilde{v}_1\tau_s} - \frac{\ln 2}{l_s^2}\left((\Delta_1 - \tilde{v}_1\tau)^2 + \Delta_2^2 + \Delta_3^2\right)\right] \tag{5}$$

Following the derivations in [19,21] assuming the compact source scale and locally parallel flow approximations are valid the final noise spectra prediction formula becomes

$$S(\mathbf{x},\omega) = \int_V \int_V A_{ijkl}(\mathbf{y}) W(\mathbf{y}) \hat{I}_{ij} \hat{I}_{kl}^* d\mathbf{y}, \tag{6}$$

where the function $W(\mathbf{y})$, which emerges as a result of the analytical integration over the correlation volume Δ, is:

$$W(\mathbf{y}) = \left(\frac{\pi}{\ln 2}\right)^{3/2} \frac{2 l_s^3 \tau_s}{1 + (\omega(1 - \tilde{v}_1 / c_\infty \cos\varphi)\tau_s)^2} \exp\left(-\frac{(\omega l_s / \tilde{v}_1)^2}{4 \ln 2}\right). \tag{7}$$

where, $\tilde{v}_1$ is the local axial jet meanflow velocity that is assumed to be equal to the eddy convection speed and

$$A_{ijkl} = C_{ijkl}(2\bar{\rho}\kappa)^2 \tag{8}$$

is the corresponding correlation amplitude.

In (7) τ_s and l_s are the acoustic time and space correlation length scales which can be computed either from the turbulent kinetic energy with the time-averaged absolute vorticity solution component [21].

$$l_s = c_\ell \sqrt{\kappa} / \xi,\ \tau_s = c_\tau / \xi, . \tag{10}$$

The turbulent kinetic energy, vorticity, meanflow velocity and other components of the acoustic analogy model are obtained from averaging the LES flow fields, thereby essentially using LES like Reynolds Averaged Navier-Stokes (RANS) flow solution.

The dimensionless parameters, c_l and c_τ are determined empirically by the best fit to the far-field noise data at 90º observer angle (and then kept fixed for all other observer angles). The generality of the acoustic length and time scale coefficients have been discussed and demonstrated in [21] for the single-stream isothermal jets and the idea in the context is to use the set of coefficients obtained for cold SILOET jet from [21] in the calculation of the acoustic spectra for Ma = 0.6 and Ma = 0.8 jets. In a similar fashion, the dimensionless coefficients C_{ijkl} used in the model (8) were previously computed from analysing the LES solution of cold SILOET jet [21].

In addition to the LES-FW-H and the acoustic analogy solutions, far-field noise spectra of the two jets are predicted using the NASA sJet model [15] for same pressure and temperature ratio conditions. sJet is an empirical model based on interpolations across a large set of NASA jet noise data. Hence, comparison with sJet solutions provides an independent reference point corresponding to a consensus NASA jet noise spectra to cross validate the numerical predictions and the Doak Laboratory measurements.

V.Far-field Noise Predictions

Figs.9 and 10 show the comparison of the far-field noise spectra results of the LES-FW-H method with the Doak Laboratory Experiment data and the sJet predictions for the Ma = 0.6 jet for 8 observer angles from 30 to 100 degrees. For 30 degrees no experimental data available, hence, the LES results are compared just with the sJet solution. Fig.11

and 12 show the same comparison, but for the Ma = 0.8 jet. The observer angle is defined relative to the jet flow axis. No averaging over the azimuthal angle is performed to cosmetically smoothen the noise spectra.

For the slower Ma = 0.6 jet, the LES solutions are within 1-2 dB from the Doak Laboratory Experiment for frequencies ranging from $St_D = 0.04$ to $St_D = 10$ for observer angles from 30 to 70 degrees. Interestingly, in comparison with the sJet predictions, which show 1-2dB differences with the Doak Laboratory Experiment data for high observer angles, the LES noise prediction remains within 1-2dB up to $St_D = 10$ over the entire range of the downstream angles, from 30º to 90º. For the upstream observer angle, 100º, where the the Doak Laboratory Experiment data are in perfect agreement with the consensus NASA model, the 1-2dB accuracy of current LES predictions is limited to $St_D = 4 - 5$, which is due to the insufficiently well-adjusted FW-H surface upstream of the nozzle exit for this low-speed jet case.

For the faster Ma = 0.8 jet, for most angles, the LES results are within 1 dB from the Doak Laboratory Experiment from $St_D = 0.04$ to $St_D = 7$ and within 2dB error up to $St_D = 8$. Capturing of the high frequency noise appears to be a less of problem for the high-speed jet case compared to the Ma = 0.6 jet. It can also be noted that there is a discrepancy at high frequencies between the Doak Laboratory Experiment dataset and the sJet model, possibly due to a Reynolds number effect. In comparison with the consensus NASA model, the Doak Laboratory Experiment underpredicts noise at $St_D = 10$ by around 3dB. Notably, in comparison with the sJet model, the LES predictions for the Ma = 0.8 case remain within 1-2dB error over the entire frequency range of $0.04 < St_D < 10$ for observer angles from 30º to 90º.

Finally, Figs. 11 and 12 compare the predictions of the reduced-order model based on the GAA model with the Doak Laboratory Experiment datasets and the sJet solutions. As discussed in the previous section, the reduced-order acoustic model is based on the LES meanflow and turbulent kinetic energy solutions without access to the detailed space-time resolved information. Therefore, in comparison with the FW-H method, the acoustic analogy model is suitable for quick turn-around-time jet noise calculations, which can be run on a personal laptop. The reduced-order model predictions are within 2-3dB agreement with the Doak Laboratory Experiment and the NASA consensus model in a range of frequencies from $St_D = 0.04$ to $St_D = 4$ for Ma = 0.6 and observer angles from 30 to 100 degrees. For the higher Mach case, Ma = 0.8 the high-frequency limitation of the acoustic reduced-order model for the mid-range angles in terms of 2-3dB accuracy reduces to $St_D = 2$. Importantly the peak noise at 40º angle is captured within 1 dB in comparison with the Doak Laboratory Experiment for both the Ma = 0.6 and Ma = 0.8 jet cases.

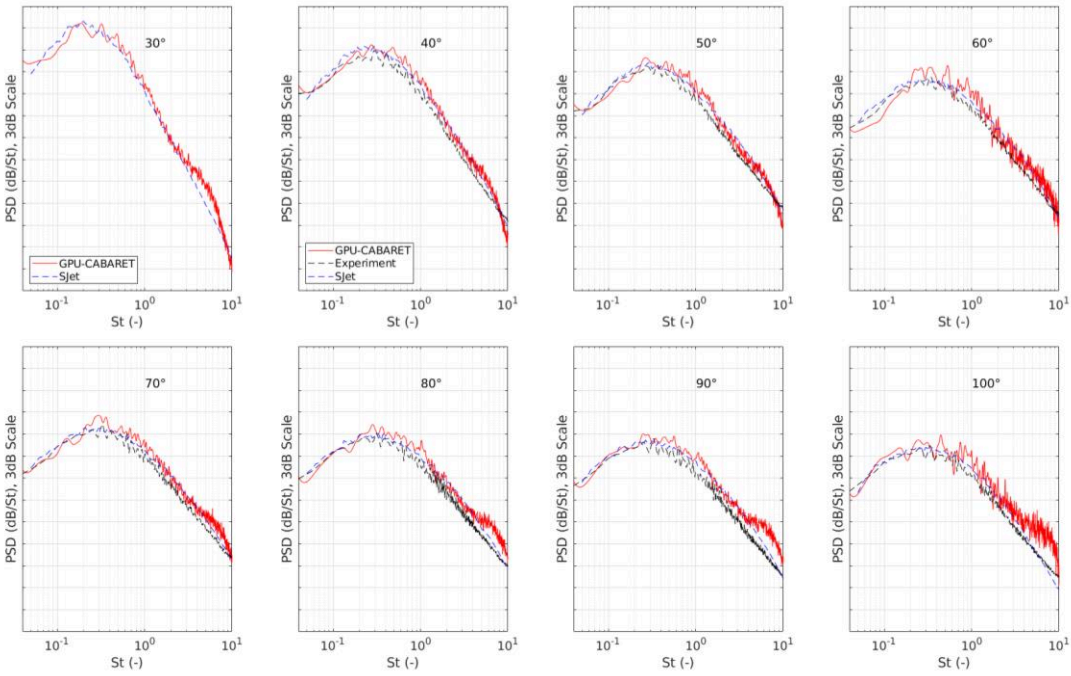

Fig.9 FW-H predictions for Ma=0.6 case. Results are for 550 TUs.

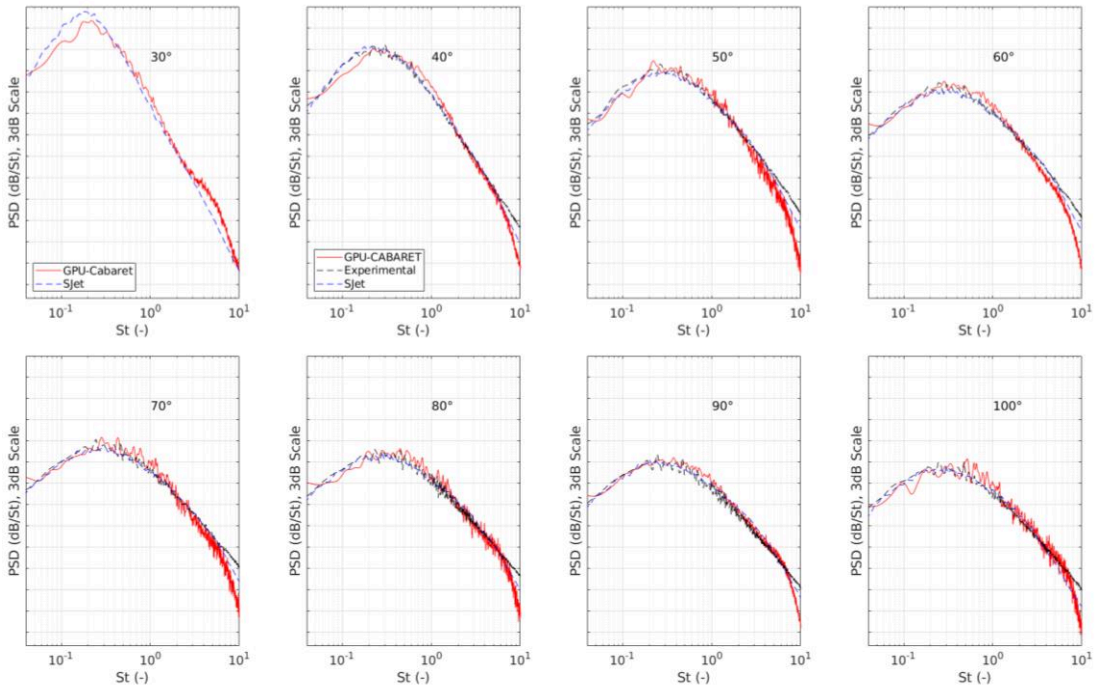

Fig.10 FW-H results for Ma=0.8 case. Results are for 1100 TUs.

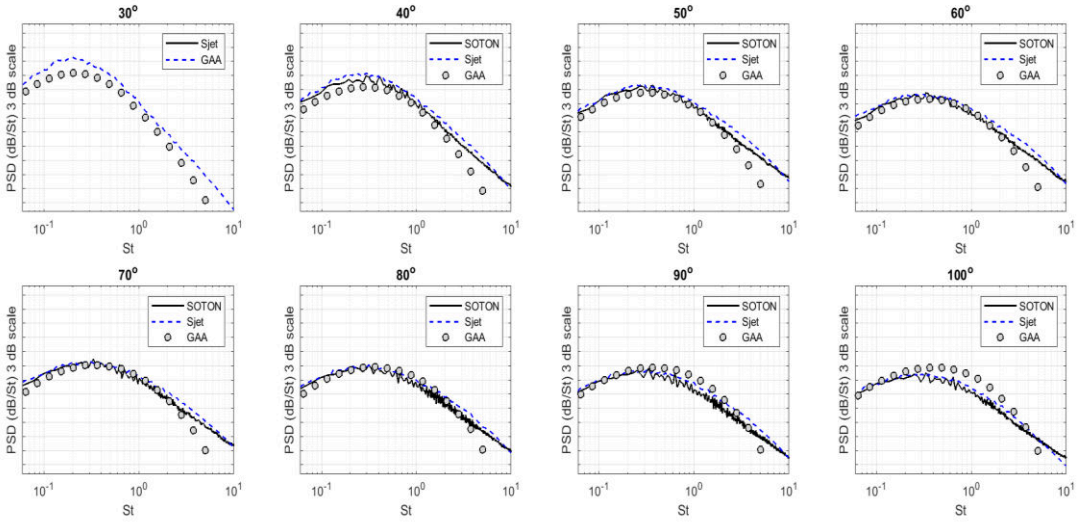

Fig.11 Far-field noise spectra for the Ma = 0.6 jet for eight polar observer angles.

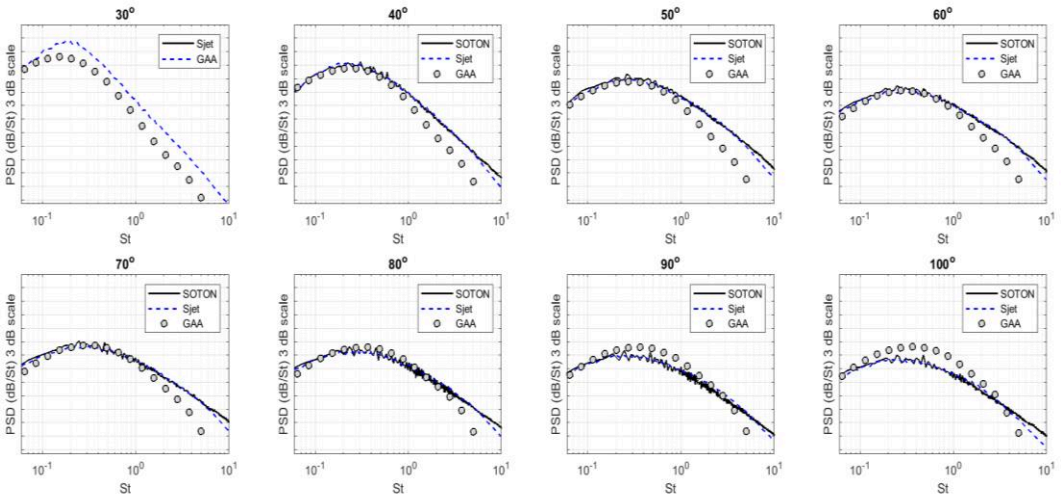

Fig.12 Far-field noise spectra for the Ma = 0.8 jet for eight polar observer angles.

Conclusions

Two cold static jet cases corresponding to the Doak Laboratory Flight Jet Rig experiment at Mach numbers 0.6 and 0.8 have been computed using the Wall Modeled Large Eddy Simulation (WMLES) method based on the high-resolution CABARET scheme. The WMLES CABARET is implemented on GPUs cards to significantly accelerate the time to solution on a workstation with 2x NVIDIA RTX A6000 GPUs for LES grids of 137-196 million cells. In comparison with previous CABARET jet flow calculations, a distinct feature of the current work is ensuring a good match between the LES solutions and the experiment for turbulent jet inflow conditions just downstream of the nozzle exit.

A generally good agreement between the LES solutions and the experiment for both the mean flow velocity and r.m.s. fluctuation of the streamwise velocity components is demonstrated for radial distributions. Some discrepancies along the jet centreline and the end of potential core are noticed, which can be related to the nature of the invasive flow measurements in the Doak experiment.

Far-field noise predictions are obtained by combining the LES solution with the permeable formulation of the Ffowcs Williams – Hawkings method including multiple closing discs. The computed noise spectra are compared with the far-field measurements of the Doak experiment as well as the predictions of the empirical sJet code, which corresponds to the NASA consensus jet noise model of the same Doak jets. Interestingly, some 2-3dB discrepancy between the Doak experiment and the NASA consensus model results are reported at high frequencies for large observer angles, potentially due to a Reynolds number effect. The GPU LES-FW-H method is shown to consistently predict noise within 1-2 dB error for the Mach 0.6 jet and 1 dB for the Mach 0.8 jet in comparison with the Doak experiment upto frequencies corresponding to the Strouhal number of 5-7 for a wide range of observer angles. The numerical solution agrees even better with the NASA consensus model for the same jet conditions. In this case the accuracy margin of the LES-FW-H model is established to be 1-2dB for the entire range of observer angles and frequencies upto to the Strouhal number based on the nozzle diameter equal to 10. It can be noted that the latter range of high frequencies is of importance for industrial applications dealing with large nozzles.

In addition, further noise predictions are made by substituting the time-averaged LES flow solutions into a reduced-order implementation of the Generalised Acoustic Analogy (GAA) model. To probe the model robustness, no additional calibrations of the GAA model are attempted in comparison with the previously established set of best dimensionless source amplitude and the acoustic length and time scale coefficients for a different high-speed jet case. Despite the lack of any calibration, noise predictions of the reduced-order GAA model show encouraging agreement with the Doak experiment upto Strouhal numbers 1.5-2 within 2-3dB accuracy for all observer angles tested. Importantly, the peak jet mixing noise at a shallow angle to the jet, which is traditionally difficult to predict for many reduced-order acoustic models, is captured by the reduced-order jet noise model within 1dB for both Mach numbers.

Acknowledgments

This work is supported by the European Union's H2020 program under the DJINN (Decrease Jet INstallation Noise) project, Grant Agreement No. 861438.

The authors thank Dr Abbas Khavaran for making his sJet code readily available.

Reference List

[1] Tanna, H. K., An Experimental Study of Jet Noise: Part I Turbulent Mixing Noise, Journal of Sound and Vibration,Vol. 50, No. XX, 1977.

[2] Bridges, J., and Wernet, M. P., The NASA Subsonic Jet Particle Image Velocimetry (PIV) Dataset, NASA TM-2011-216807, 2011

[3] Lawrence, J., and Self, R., Installed Jet-Flap Impingement Tonal Noise, 21st AIAA/CEAS Aeroacoustics Conference, AIAA Paper 2015-3118, 2015. https://doi.org/10.2514/6.2015-3118;

[4] Proença, A., Lawrence, J., and Self, R., Measurements of the Single-Point and Joint Turbulence Statistics of High Subsonic Jets Using Hot-WireAnemometry, Experiments in Fluids, Vol. 60, No. 4, 2019, p. 63. https://doi.org/10.1007/s00348-019-2716-3

[5] Proença, A. R., Lawrence, J. L. T., and Self, R. H. Experimental Investigation into the Turbulence Flowfield of In-Flight Round Jets. AIAA Journal, American Institute of Aeronautics and Astronautics (AIAA), 58, 8, Aug, 2020, pp. 3339–3350

[6] Goloviznin, V. M., Samarskii, A. A., Finite difference approximation of convective transport equation with space splitting time derivative, Jour Matem. Mod., 1998 , 10(1), 86–100

[7] Karabasov, S. A., and Goloviznin, V. M., Compact Accurately Boundary Adjusting high-REsolution Technique for Fluid Dynamics, J. Comput. Phys., 2009, 228, 7426-7451

[8] Chintagunta, A., Naghibi, S.E., and Karabasov, S.A. Flux-corrected dispersion-improved CABARET schemes for linear and nonlinear wave propagation problems, Computers & Fluids, August 2017

[9] Semiletov, V. A., and Karabasov, S. A., CABARET scheme with conservation-flux asynchronous time-stepping for nonlinear aeroacoustics problems, Journal of Computational Physics, 2013, 253(15), 157165

[10] Markesteijn, A. P., Semiletov, V., and Karabasov, S. A. GPU CABARET Solutions for the SILOET Jet Noise Experiment: Flow and Noise Modelling. 22nd AIAA/CEAS Aeroacoustics Conference, American Institute of Aeronautics and Astronautics, May 27, 2016

[11] Markesteijn, A.P., Karabasov, S. A., GPU-CABARET Solutions for the NASA SHJAR Jet Noise Experiment: Flow and Noise Modeling, 23rd AIAA/CEAS Aeroacoustics Conference, 2017. https://doi.org/10.2514/6.2017-3852

[12] Markesteijn, A.P., Karabasov, S.A., CABARET solutions on graphics processing units for NASA jets: Grid sensitivity and unsteady inflow condition effect, Comptes Rendus Mécanique, Vol. 346 (10), pp. 948-963, 2018. https://doi.org/10.1016/j.crme.2018.07.004

[13] Markesteijn, A.P., Gryazev, V., Karabasov, S.A., Ayupov, R.Sh., Benderskiy, L. A., Lyubimov, D.A. Flow and Noise Predictions of Coaxial Jets, AIAA Journal, Vol. 58(12), 2020. https://doi.org/10.2514/1.J058881.

[14] Ffowcs Williams, J. E., Hawkings, D. L., Sound generation by turbulence and surfaces in arbitrary motion, Philosophical Transactions of The Royal Society A, Vol. 264, 1969, 32142. https://doi.org/10.1098/rsta.1969.0031

[15] Khavaran, A., Bridges, J., Development of Jet Noise Power Spectral Laws Using SHJAR Data, 30th AIAA Aeroacoustics Conference (2009) 3378. doi:10.2514/6.2009-3378

[16] Goldstein, M.E., A unified approach to some recent developments in jet noise theory, International Journal of Aeroacoustics, Vol.1, pp. 1-16, 2002. https://doi.org/10.1260/1475472021502640

[17] Goldstein, M.E., A generalized acoustic analogy, Journal of Fluid Mechanics, Vol. 488, 2003, pp. 315-333. https://doi.org/10.1017/S0022112003004890.

[18] Goldstein, M.E., Leib, S. J., The Aero-acoustics of slowly diverging supersonic jets, Journal of Fluid Mechanics., Vol. 600, 2008. https://doi.org/10.1017/S0022112008000311

[19] Karabasov, S.A., Afsar, M.Z., Hynes, T.P., Dowling, A.P., McMullan, W.A., Pokora, C.D., Page, G.J. and McGuirk, J.J., Jet Noise: Acoustic Analogy informed by Large Eddy Simulation, AIAA J., 2010. 48(7), 1312-1325

[20] Depuru Mohan, N.K., Dowling, A.P., Karabasov, S.A., Xia, H., Graham, O. Hynes, T.P., Tucker, P.G., Acoustic sources and far-field noise of chevron and round jets, AIAA Journal, Vol. 53(9), 2015. https://doi.org/10.2514/1.J052973

[21] Gryazev, V., Markesteijn, A.P., Karabasov, S.A., "Generalised acoustic analogy modelling of hot jet noise" *AIAA Journal*, 2021.
[22] Park, G.I. 2015. "Wall-modeled large-eddy simulation of a separated flow over the NASA wall-mounted hump", Center for Turbulence Research, Annual Research Briefs
[23] Saad, T. Cline, D., Stoll, R. and Sutherland, J.C. 2014. Scalable Tools for Generating Synthetic Isotropic Turbulence with Arbitrary Spectra. http://dx.doi.org/10.2514/1.J055230.
[24] Richards, A., Saad, T. and Sutherland, J.C. 2018. A Fast Turbulence Generator using Graphics Processing Units", AIAA AVIATION Forum, (AIAA 2018-3559). https://doi.org/10.2514/6.2018-3559
[25] Mukha, T., Rezaeiravesh, S. and Liefvendahl, M. 2018. "A Library for Wall-Modelled Large-Eddy Simulation Based on OpenFOAM Technology."
[26] Brès, G.A. Jordan, P., Jaunet, V., Rallic, M. Le., Cavalieri, A.V.G., Towne, A., Lele, S.K., Colonius, T., Schmidt, O.T., Importance of the nozzle-exit boundary-layer state in subsonic turbulent jets, Journal of Fluid Mechanics, 2018, 851, 83-124
[27] Shur, M. L., Spalart, P. R., and Strelets, M. K., "Noise Prediction for Increasingly Complex Jets. Part I: Methods and Tests," International Journal of Aeroacoustics, Vol. 4, No. 3, 2005, pp. 213–245. https://doi.org/10.1260/1475472054771376
[28] Tam, C.K.W., Auriault, L., "Mean flow refraction effects on sound from localized sources in a jet," *Journal of Fluid Mechanics*, Vol. 370, pp. 149-174, 1998. https://doi.org/10.1017/S0022112098001852.
[29] Tam, C. K. W., Auriault, L., (1999). "Jet Mixing Noise from Fine-Scale Turbulence." AIAA Journal, Vol. 37, No. 2, pp.145-153

Flow and noise predictions of the isolated subsonic jets from the Doak Laboratory experiment

Gryazev, Vasily

2022-06-13

Gryazev V, Markesteijn AP, Karabasov SA, et al., (2022) Flow and noise predictions of the isolated subsonic jets from the Doak Laboratory experiment. In: 28th AIAA/CEAS Aeroacoustics 2022 Conference, 14-17 June 2022, Southampton, UK. Paper number AIAA 2022-2935
https://doi.org/10.2514/6.2022-2935